



Effect of processing conditions on the structure and collective magnetic properties of flowerlike nickel nanostructures

Chunhong Gong^{a,b}, Juntao Tian^a, Jingwei Zhang^{a,*}, Xuefeng Zhang^c, Laigui Yu^a, Zhijun Zhang^{a,*}

^a Key Laboratory of Special Functional Materials of Ministry of Education, Henan University, Kaifeng 475004, China

^b College of Chemistry and Chemical Engineering, Henan University, Kaifeng 475004, China

^c Industrial Materials Institute, National Research Council Canada, Quebec J4B 6Y4, Canada

ARTICLE INFO

Article history:

Received 7 July 2009

Received in revised form 3 February 2010

Accepted 2 March 2010

Available online 9 March 2010

Keywords:

A. Metals

B. Magnetic materials

C. Chemical synthesis

D. Magnetic properties

ABSTRACT

To acquiring more insights into the relationship between the morphology and magnetic properties of magnetic nanocrystallites, uniform flowerlike Ni nanostructures with different branch lengths were fabricated via a simple solvothermal reduction route based on a series of comparative experiments. The formation mechanism of the Ni flowers was proposed. Moreover, the magnetic properties of the products were evaluated. Results indicate that the morphology of the Ni particles strongly depends on reaction temperature, and the branch length of the flowerlike Ni particles strongly depends on the initial concentration of Ni²⁺ ions. The flowerlike Ni particles with a longer branch length show higher coercivity value, which may be attributed to the peculiar microstructure. We believe the present research may provide an ideal example for the synthesis of assembled magnetic nanostructures with controllable morphology and magnetic properties.

© 2010 Elsevier Ltd. All rights reserved.

1. Introduction

It is well-known that nanoscale magnetic materials have potential applications in areas such as electromagnetic wave shielding or/and absorbance, magnetic fluids, magnetic recording devices, and magnetic drug delivery [1]. Since the magnetic properties of magnetic nanocrystals depend strongly on structure and morphology, it is imperative to study novel shape-controlling synthetic strategies and hence fabricate novel magnetic nanostructures with unusual properties [2]. So far, a large number of magnetic nanostructures with peculiar shapes and magnetic properties have been successfully fabricated [3–6]. To name a few, various shape-controllable Ni nanostructures, e.g., Ni nanowires electrodeposited on anodic aluminum oxide (AAO) templates [3], Ni nanobelts grown with the assistance of complexing agents and surfactants [4], Ni hollow spheres formed on microemulsion template [5], and Ni nanorods created by thermal decomposition of organic compounds have been fabricated using different precursors and routes [6].

Several theories are currently available for analyzing shape-dependent magnetic properties, and it has been widely recognized that magnetic particles with large shape anisotropy usually have a

larger coercivity (H_c) than common materials [7,8]. However, it still remains a challenge to efficiently and conveniently control the morphology of anisotropy magnetic nanostructures. In a previous research we prepared one dimensional (1D) Ni nanocrystallite fibers with different lengths using magnetic field-induced self-assembly and found that a relatively high intensity of the magnetic field and large concentration of Ni²⁺ ions favored the generation of Ni fibers with increased length and magnetic properties [9]. Unfortunately, there have been very few reports on the fabrication of three dimensional (3D) nickel nanostructures as a kind of important shape anisotropy materials [10–12], possibly because complicated multi-step processes are usually involved and it requires rigorous conditions such as high temperature and use of surfactants and/or external magnetic field to effectively tailor the size and morphology of the products. In other words, it also remains a challenge to develop simple and reliable routes for the self-assembly of magnetic nanoparticles with controllable multi-dimensional morphology.

With those perspectives in mind, by properly adjusting reaction conditions, 3D flowerlike Ni particles with different branch lengths were successfully prepared via a convenient solvothermal process in the absence of any surfactants or external magnetic forces. The magnetic properties of the products at room temperature were systemically evaluated. Hopefully, the present research is to provide some insights into the relationship between the morphology and magnetic properties of Ni nanostructures.

* Corresponding authors.

E-mail address: jwzhang0378@yahoo.cn (J. Zhang).

2. Experimental

All reagents are of analytical grade and used without further purification. In a typical experiment, an appropriate amount of nickel chloride ($\text{NiCl}_2 \cdot 6\text{H}_2\text{O}$) (0.01–0.10 M) was dissolved directly in 30 mL of ethylene glycol. Then 3 mL of ammonia solution (25–28 wt%) and 3 mL of hydrazine hydrate solution ($\text{N}_2\text{H}_4 \cdot \text{H}_2\text{O}$, 80 wt%) were added into the above solution under continuous stirring, allowing the generation of a red mixture. Finally, the red mixture was transferred into a 50-mL Teflon-lined autoclave and sealed and held at 90–150 °C for 7 h, followed by cooling to room temperature. The reactions can be described as follows:



where Ni^{2+} ions are reduced into Ni and the evolved nitrogen can help to prevent nascent nickel nanocrystallites from oxidation.

The as-synthesized solid products were precipitated, separated, washed with ethanol for several times, and dried in a vacuum oven at 60 °C for 24 h. The structure and morphology of the resultant dried samples were characterized by means of X-ray diffraction (XRD, Philips X' Pert Pro X-ray diffractometer; $\text{Cu-K}\alpha$ radiation, $\lambda = 0.15418$ nm), scanning electron microscopy (SEM, JEOL JSM-5600LV; acceleration voltage of 20 kV), field-emission scanning electron microscopy (FESEM, Hitachi FE-SEM, S-4800; carried out with a field-emission scanning electron microanalyzer (JEOL-6300F, 15 kV)), and transmission electron microscopy (TEM, JEOL JEM-2010; accelerating voltage 200 kV). The main constituent elements of the typical products were also determined by means of energy-dispersive X-ray spectrometry (EDS) attached to the SEM (JEOL JSM-5600LV). The magnetic hysteresis loops ($M-H$ loops) of the products at room temperature were measured using a vibrating sample magnetometer (Lake Shore 7410 VSM, USA).

3. Results and discussion

As a typical example, the sample obtained via the solvothermal process of 0.10 M Ni^{2+} and 3 mL of ammonia solution and 3 mL of hydrazine at 100 °C for 7 h was analyzed by using FESEM and TEM, and the results are shown in Fig. 1. It is seen that the flowerlike Ni particles have a diameter of 4–6 μm and show good uniformity (see Fig. 1(a)). At the same time, the flowery particle consists of a sphere-like core attached to various nanostructure branches, and most of the branches have radiating arrangement around the core. Such structural features are also reflected in corresponding TEM image (Fig. 1(b)). Moreover, the TEM image of an individual branch of the flowerlike particles shows signs of tapering off from top to bottom of a tip (Fig. 1(c)). And it is likely that the branch has a length of about 1 μm and width from several nanometers to about 200 nm. Fig. 1d shows a typical selected area electron diffraction (SAED) pattern obtained along a typical individual branch. The spots pattern indicates that the as-prepared Ni sample has single crystalline structure and can be indexed to pure cubic phase nickel.

Fig. 2 shows the typical XRD and EDS spectra of the as-prepared 3D Ni nanostructures obtained under the same conditions as in Fig. 1. The XRD pattern shows obvious signs of broadening, indicating that the as-prepared Ni sample may consist of nanocrystallites (Fig. 2a). Besides, the XRD pattern can be indexed as face-centered cubic (fcc) nickel (JCPDS 01-1260) [13]. Although it is conceivable that Ni nanostructures are very active and might react with oxygen in air forming oxides, no nickel oxide or any other impurities have been detected by XRD, which indicates that nickel crystalline fabricated under the present conditions has a very high purity. Moreover, the EDS spectrum (Fig. 2b) also illustrates that the products contain only nickel, which corresponds well to the SAED pattern shown in Fig. 1(d).

It is well-known that the morphology of Ni nanostructures is highly dependent on many factors such as temperature, concentration of reactants, and the types of solvents and surfactants, etc.

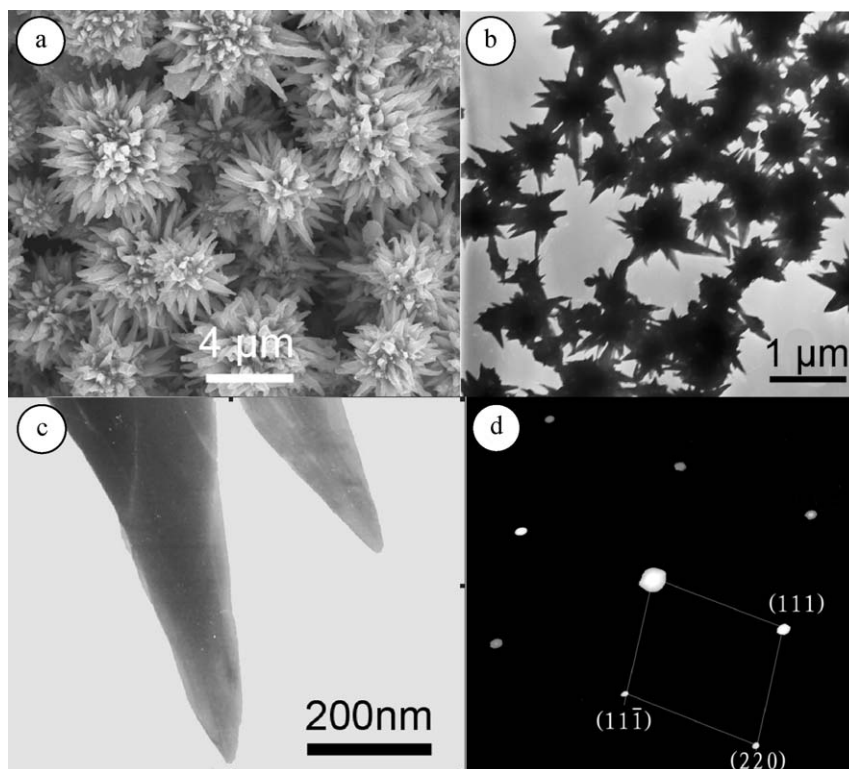


Fig. 1. FESEM image of Ni flowerlike sample (a); TEM images of the Ni flowerlike sample (b) and the Ni branch (c); and SAED pattern of a Ni branch (d).

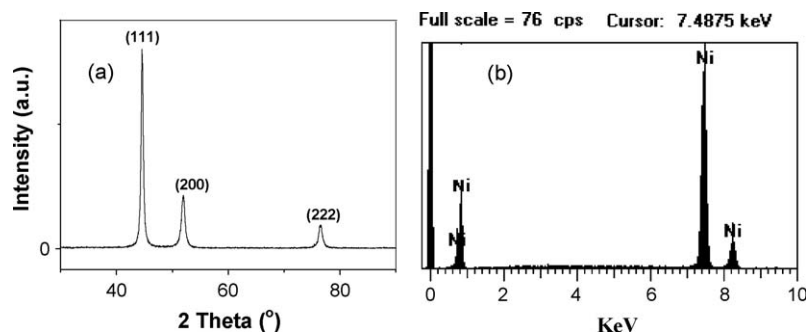


Fig. 2. XRD (a) and EDS (b) spectra of as-prepared 3D Ni nanostructures obtained under the same conditions as in Fig. 1.

For example, we recently found that the microstructure of Ni nanocrystallites was closely dependent on the type of the solvents and only alcohol-type solvents containing double hydroxyl groups might be helpful to the formation of Ni nanocrystallites with shape anisotropy [14]. To further understand the self-organization mechanism and growth process of flowerlike Ni nanostructures, the products obtained at different parameters were investigated in detail. This, hopefully, is to help to shed light on the relationship among the morphology of Ni nanostructures and the concentration of initial Ni^{2+} ions and reaction temperature as well.

In order to investigate the effect of the concentration of Ni^{2+} ions on the morphology of Ni products, the reduction of Ni^{2+} ions with varied initial concentration from 0.01 M to 0.10 M by 3 mL of hydrazine hydrate solution in the presence of 3 mL of ammonia solution was performed at 100 °C. Fig. 3 shows the SEM images of the resulting Ni products. It is clearly seen that the morphology of the Ni products is highly dependent on the initial concentration of Ni^{2+} ions. The Ni sample obtained at an initial Ni^{2+} ions concentration of as low as 0.01 M appears as microspheres, showing relatively smooth surface and non-uniform size of 0.2–2 μm (Fig. 3(a)). When the initial concentration of Ni^{2+} ions is higher than 0.01 M, Ni nanostructures with 3D flowerlike morphology is obtained and the branch length of the flowerlike particles gradually increases with increasing initial concentration of Ni^{2+} ions (Fig. 3(b–d)). By carefully viewing the magnified SEM

images, it can be seen that the three samples prepared at Ni^{2+} ion concentration of 0.02 M, 0.06 M, and 0.10 M (see the insets in Fig. 3(b–d)) have typical branches length of 100–300 nm, 300–600 nm, and 800–1500 nm, respectively. Moreover, it is likely that a higher concentration of Ni^{2+} ions, for instance, 0.06 M and 0.10 M, is beneficial to the formation of flowerlike particles with longer branches (see Fig. 3(c–d)).

The precursor might play a very important role in terms of the morphology of the Ni nanostructures, and the above observations could be rationally understood by taking into account the influence of reduction rate on the nucleation and typical Ostwald ripening progress. In the Ostwald ripening process, the larger particles will grow at the cost of the small ones due to the difference of energy between large and small particles of a higher solubility based on the Gibbs–Thompson law [15]. Namely, in the first step, Ni^{2+} ions can form complex precursors $\text{Ni}(\text{NH}_3)_6^{2+}$ and $\text{Ni}(\text{N}_2\text{H}_4)_x^{2+}$ in solution containing ammonia and hydrazine, leading to a sharp decrease in the concentration of free Ni^{2+} ions. Subsequently, Ni complex precursors were slowly dissolved and reduced by hydrazine hydrate forming Ni atoms. Since a minimum number of atoms are required to form a stable nucleus and a collision must occur among several atoms during nucleation, the atoms formed at that period might participate mainly in collisions with already formed nuclei, instead of forming new nuclei [16]. This would result in precipitation of nuclei and their quick growth into

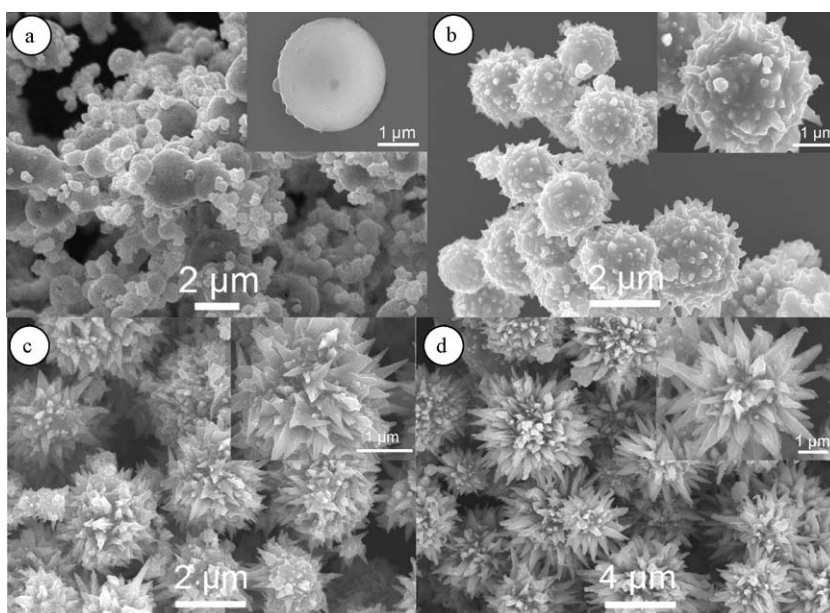


Fig. 3. SEM images of the samples obtained at 100 °C from the reaction systems with different concentrations of Ni^{2+} ions: (a) 0.01 M, (b) 0.02 M, (c) 0.06 M, and (d) 0.10 M. The insets are higher magnification images.

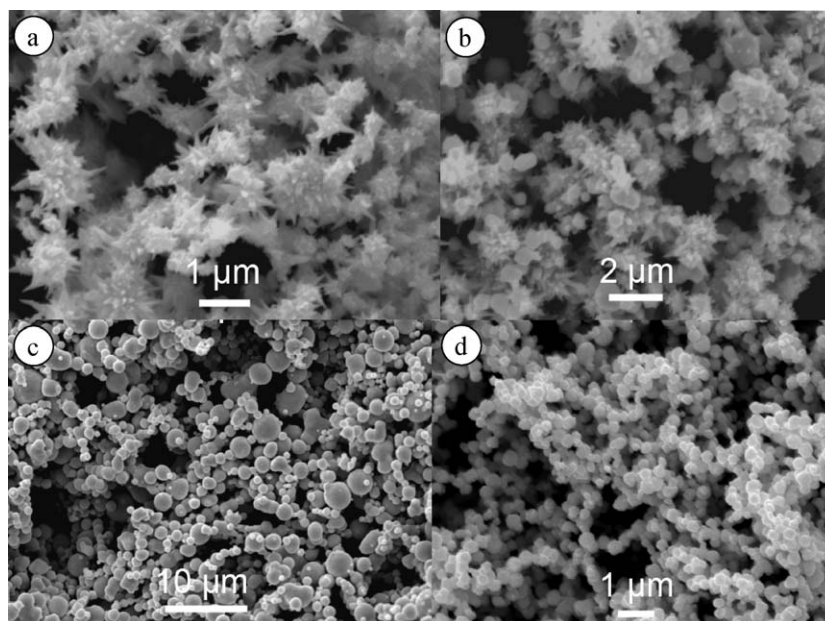


Fig. 4. SEM images of Ni samples obtained at different reaction temperature: (a) 90 °C, (b) 120 °C, (c) 130 °C, and (d) 150 °C.

primary particles. In the follow-up step, the primary particles might serve as nucleation sites of the 3D structure and finally form flowerlike structure by way of Ostwald ripening of Ni atoms and nanoparticles. Without a preferential tropism, Ni branches could grow in any directions, and subsequently, 3D flowerlike nickel nanostructures were harvested at an extended reaction time. And the branch length of the 3D nanostructures increased with increasing reaction time until the metal salt was completely consumed. Therefore, the higher the concentration of free Ni^{2+} ions, the longer the branches of the 3D nanostructures.

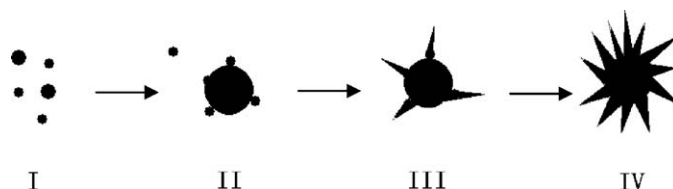
To investigate the effect of reaction temperature on the morphology of Ni products, we carried out temperature-dependent experiments with a fixed initial concentration of Ni^{2+} ions (0.10 M), 3 mL of ammonia solution, and 3 mL of hydrazine hydrate solution within a solvothermal temperature range of 90–150 °C.

The typical SEM morphologies of four samples obtained at different solvothermal temperature are shown in Fig. 4. At a lower temperature, e.g., 90 °C, a mixture of black product and blue stuff was obtained even after an extended reaction time of more than 7 h, implying that the reducing reaction could not be completed. The corresponding black product obtained by magnetic separation methods, a mixture of flowerlike particles and erose structure with spiked morphology, has a mean diameter of about 1 μm (Fig. 4(a)). At 120 °C, the product is a mixture of submicrometer-sized spheres and rough structure with spiked morphology and it has a mean diameter of about 1 μm (Fig. 4(b)). At a higher reaction temperature of 130 °C, microspheres with a relatively smooth surface were obtained, and the Ni particulates had non-uniform size of 0.5–3 μm (Fig. 4(c)). When the temperature was further increased to 150 °C, the reaction could be completed within an hour, resulting in uniform smooth Ni microspheres with a diameter of about 0.5 μm (Fig. 4(d)), which could be attributed to a faster reaction rate thereat. It seems that a moderate reaction temperature favors the formation of Ni nanostructures with good uniformity. In other words, only when the reaction temperature was fixed at 100 °C, well-defined flowerlike particles were harvested (Fig. 1). And once the reaction temperature was over 100 °C, the flowerlike morphology was destroyed.

The above-mentioned results might be explained as follows. At a lower temperature (90–120 °C), Ni complex precursors were dissolved and reduced by hydrazine hydrate slowly, leading to a

slower reduction rate. At the same time, ethylene glycol solution with a high viscosity largely restrains the diffusion of Ni nuclei, which facilitates the aggregation of Ni crystals and growth of anisotropic dendritic crystal in the early period of reduction (Fig. 4(a–b)). With the increase of temperature, the viscosity of the reaction solution was decreased and the reduction rate increased, favoring the generation of more nuclei and formation of smaller Ni spherical particles. Moreover, due to Ostwald ripening, more energy can be provided to the reaction system at a higher temperature, which also favors the re-dissolving of anisotropic dendritic crystals, resulting in spherical particles with smooth surfaces (Fig. 4(c–d)). Therefore, aside from the great dependence of branch length of Ni nanostructures on the concentration of Ni^{2+} ions, the flowerlike morphology of the Ni nanostructures also strongly depends on the reaction temperature.

The formation processes of the 3D flowerlike Ni particles are schematically illustrated in Scheme 1. In the initial stage of solvothermal reaction, Ni complex precursor $\text{Ni}(\text{NH}_3)_6^{2+}$ and $\text{Ni}(\text{N}_2\text{H}_4)_x^{2+}$ are formed and reduced into small nickel nanocrystals in the presence of hydrazine hydrate as the reducing agent (stage I). In the second stage, small nickel nanocrystals grow into Ni nuclei, providing favorable environment for the nucleation and growth of more nickel nanocrystals (stage II). In the third stage, nickel nanocrystals are gradually attached with each other to generate spherical particles, accompanied by the formation of spearlike branches via seed-induced growth (stages II and III), and



Scheme 1. Schematic illustration of the morphological evolution process of Ni flowerlike nanostructures: (I) Small nickel nanocrystals were formed from Ni precursors. (II) Small nickel nanocrystals were gradually attached with each other to generate bigger spherical nickel nanoparticles, accompanied by the formation of spearlike branches via seed-induced growth. (III) Spherical nickel particles were partially transformed into flowers with the reduction of Ni^{2+} . (IV) Nickel flowers emerged as the final product.

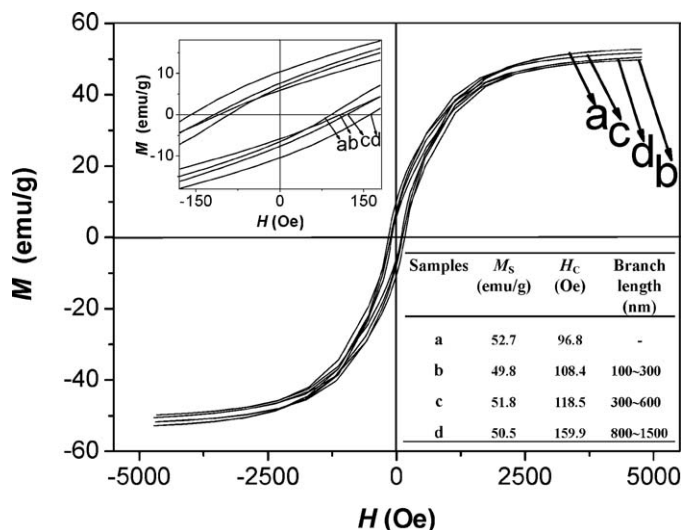


Fig. 5. Hysteresis loops at room temperature for the samples obtained at 100 °C from the reaction systems with different concentrations of Ni^{2+} ions: (a) 0.01 M, (b) 0.02 M, (c) 0.06 M, and (d) 0.10 M. The upper left inset shows the hysteresis loops of the four samples between -150 and 150 Oe. Magnetic properties of the four samples and the branch lengths of the three flowerlike samples are summarized in the lower right inset.

the length of the branches is dominated by the Ni^{2+} ions concentration. Finally, Ni flowers emerge at extended reaction duration (stage IV). However, due to the complex growth conditions involved, the detailed mechanism for the formation of final Ni nanostructures still remains unknown. And in particular, the growth process of the Ni branches can hardly be well described herewith. This is because, aside from the Ostwald ripening and diffusion, several other factors, including electrostatic and/or magnetic dipolar attraction, van der Waals forces, and so on, may also affect the self-assembly [17]. Thus further work is needed to reveal the self-assembly growth mechanism of the Ni nanostructure.

It is known that the magnetic properties of nanomaterials are closely related to size, morphologies, crystallinity, and so on. To investigate the influence of microstructure on the magnetic properties, the magnetic properties of four samples (The same as those shown in Fig. 3) were evaluated using a vibrating sample magnetometer. The M - H loops measured at room temperature are shown in Fig. 5, where the upper left inset is the magnified hysteresis loops measured at a low intensity of applied magnetic field and the saturated magnetization (M_S) and coercivity (H_C) values are listed in lower-right inset. The hysteresis loops show ferromagnetic behavior with a saturation magnetization of 49.8–52.7 emu/g, which is slightly smaller than 55 emu/g, that of the corresponding bulk material [9]. Due to the decrease in particle size, the surface-disordered layer could serve as a nonmagnetic layer and decrease the value of M_S [18]. Moreover, the use of ethylene glycol might result in the formation of a protective layer on the particle surface, and the electron exchange between ligand and surface atoms might quench the magnetic moment, both leading to decrease of M_S [10].

Usually, a moderate coercivity is desired for a magnetic medium [18]. The H_C value of the sample obtained at a lower Ni^{2+} ions concentration (0.01 M) is only 96.8 Oe (spherical shape particles), which is slightly smaller than 100 Oe, that of the corresponding bulk material [9]. The 3D flowerlike Ni nanostructures obtained at a higher Ni^{2+} ions concentration (0.02 M and above) have increased H_C with increasing branch length. Namely, when the branch length of flowerlike structure is 100–300 nm, 300–600 nm, and 800–1500 nm, the corresponding H_C value is

108.4 Oe, 118.5 Oe, and 159.9 Oe, respectively. Since the branches have higher shape anisotropy than spherical particles, the increase of H_C with increasing branch length might be attributed to the presence of a hierarchical structure which changes the magnetization reversal mechanism [19]. This conforms well to what have been reported elsewhere in that the samples with high shape anisotropy often possess high coercivity [7–13]. In addition, our experimental result gives a hint that Ni^{2+} concentration has an obvious effect on the morphologies and magnetic properties of nanocrystallites Ni products. And the improved magnetic properties of the 3D flowerlike Ni nanostructures may be very valuable to their application in magnetic recording materials.

4. Conclusions

A simple solvothermal route has been established to prepare flower-shaped nickel nanostructures in ethylene glycol in the absence of templates or expensive precision equipments. It has been found that the assembly process and morphology of the Ni nanostructures are highly dependent on the reaction conditions. By properly controlling the concentration of Ni^{2+} ions and solvothermal temperature, flowerlike Ni nanostructure and Ni microspheres are readily obtained, and it is feasible to adjust the branch length of the flowerlike particles within 200–1500 nm. The H_C value of the 3D Ni nanostructures increases with increasing branch length, which may be closely related to the unique flowery shape and is critical to the application of Ni crystallites in magnetic recording, catalysis, conduction, etc. Hopefully, the present synthetic method is to be accepted as an efficient model for preparing magnetic assembly nanostructures with controllable morphology and magnetic properties via simply controlling reaction conditions. And it may be an ideal model for acquiring more insights into the relationship between the morphologies and magnetic properties of Ni nanostructures.

Acknowledgments

We acknowledge financial support from the National Basic Research Program of China (project of “973” Plan, grant No. 2007CB607606) and National Science Foundation of China (Grant Nos. 50902045/E0213 and 20971037/B0111).

References

- [1] (a) X.F. Zhang, X.L. Dong, H. Huang, B. Lv, J.P. Lei, C.J. Choi, *J. Phys. D: Appl. Phys.* 40 (2007) 5383–5387; (b) C.H. Gong, Y.P. Duan, J.T. Tian, Z.S. Wu, Z.J. Zhang, *J. Appl. Polym. Sci.* 110 (2008) 569–577; (c) G. Leem, S. Sarangi, S. Zhang, I. Rusakova, A. Brazdeikis, D. Litvinov, T.R. Lee, *Cryst. Growth Des.* 9 (2009) 32–34; (d) M.P. Pileni, *Adv. Funct. Mater.* 11 (2001) 323–336; (e) V.F. Puentes, K.M. Krishnan, A.P. Alivisatos, *Science* 291 (2001) 2115–2117.
- [2] Y. Sahoo, M. Cheon, S. Wang, H. Luo, E.P. Furlani, P.N. Prasad, *J. Phys. Chem. B* 108 (2004) 3380–3383.
- [3] (a) I.Z. Rahman, A. Boboc, K.M. Razeeb, M.A. Rahman, *J. Magn. Magn. Mater.* 290–291 (2005) 246–249; (b) K.S. Napolskii, A.A. Eliseev, N.V. Yesin, A.V. Lukashin, Y.D. Tretyakov, N.A. Grigorieva, S.V. Grigoriev, H. Eckerlebe, *Physica E* 37 (2006) 178–183.
- [4] Z.P. Liu, S. Li, Y. Yang, S. Peng, Z.K. Hu, Y.T. Qian, *Adv. Mater.* 15 (2003) 1946–1948.
- [5] (a) J.C. Bao, Y.Y. Liang, Z. Xu, L. Si, *Adv. Mater.* 15 (2003) 1832–1835; (b) Q. Liu, H.J. Liu, M. Han, J.M. Zhu, Y.Y. Liang, Z. Xu, Y. Song, *Adv. Mater.* 17 (2005) 1995–1999.
- [6] N. Cordente, M. Respaud, F. Senocq, M. Casanove, C. Amiens, B. Chaudret, *Nano Lett* 1 (2001) 565–568.
- [7] (a) Y. Soumare, J.Y. Piquemal, T. Maurer, F. Ott, G. Chaboussant, A. Falquic, G. Viau, *J. Mater. Chem.* 18 (2008) 5696–5702; (b) X.M. Liu, S.Y. Fu, *J. Cryst. Growth* 306 (2007) 428–432; (c) J.C. Bao, C.Y. Tie, Z. Xu, Q.F. Zhou, D. Shen, Q. Ma, *Adv. Mater.* 13 (2001) 1631–1633.
- [8] R.H. Wang, J.S. Jiang, M. Hu, *Mater. Res. Bull.* 44 (2009) 1468–1473.
- [9] C.H. Gong, L.G. Yu, Y.P. Duan, J.T. Tian, Z.S. Wu, Z.J. Zhang, *Eur. J. Inorg. Chem.* (2008) 2884–2891.

- [10] G.Q. Zhang, T. Zhang, X.L. Lu, W. Wang, J.F. Qu, X.G. Li, *J. Phys. Chem. C* 111 (2007) 12663–12668.
- [11] X.M. Ni, Q.B. Zhao, D.E. Zhang, X.J. Zhang, H.G. Zheng, *J. Phys. Chem. C* 111 (2007) 601–605.
- [12] (a) X.M. Ni, Q.B. Zhao, H.G. Zheng, B.B. Li, J.M. Song, D.E. Zhang, X.J. Zhang, *Eur. J. Inorg. Chem.* (2005) 4788–4793;
(b) F.L. Jia, L.Z. Zhang, X.Y. Shang, Y. Yang, *Adv. Mater.* 20 (2008) 1050–1054.
- [13] C.H. Gong, J.T. Tian, T. Zhao, Z.S. Wu, Z.J. Zhang, *Mater. Res. Bull.* 44 (2009) 35–40.
- [14] C.H. Gong, C.Q. Du, Y. Zhang, Z.S. Wu, Z.J. Zhang, *Chin. J. Inorg. Chem.* 25 (2009) 1569–1574.
- [15] G.S. Guo, F.B. Gu, Z.H. Wang, H.Y. Guo, *Chin. Chem. Lett.* 16 (2005) 1101–1104.
- [16] S.H. Wu, D.H. Chen, *J. Colloid. Interf. Sci.* 259 (2003) 282–286.
- [17] C.H. Gong, J.T. Tian, Z.S. Wu, Z.J. Zhang, *Chin. J. Inorg. Chem.* 24 (2008) 964–970.
- [18] A.H. Lu, E.L. Salabas, F. Schüth, *Angew. Chem. Int. Ed.* 46 (2007) 1222–1244.
- [19] L.L.P. Diandra, D.R. Reuben, *Chem. Mater.* 8 (1996) 1770–1783.